Transition between different regimes of rf glow discharges

Ph. Belenguer and J. P. Boeuf
Centre de Physique Atomique de Toulouse, Université Paul Sabatier, 118 route de Narbonne, 31062 Toulouse CEDEX, France
(Received 30 October 1989)

A self-consistent fluid model of radio-frequency glow discharges has been used to analyze the existence of two different discharge regimes and the transition between them. The existence of these regimes had been previously established by Levitskii [Sov. Phys. Tech. Phys. **2**, 887 (1958)]. The self-sustaining and power-deposition mechanisms that characterize each of these regimes are drastically different. In the first regime, termed as the "wave-riding regime" corresponding to low discharge power, most of the power deposition is due to bulk plasma electrons heated by the sheath expansions. In the second regime termed as the "secondary electron regime" corresponding to higher discharge power, the discharge is sustained mainly by electrons emitted by the electrodes under ion bombardment and avalanching in the sheath regions. The numerical results are in good agreement with previous experimental measurements by Godyak and Kanneh [IEEE Trans. Plasma Sci. **PS-14**, 112 (1986)]. The results presented in this paper form the first self-consistent description of these different regimes and of the transition between them. The validity domain of the model is restricted to pressure higher than a fraction of Torr and frequency less than a few tens of MHz. The gas being considered is helium and the discharge power varies between 0 and 700 mW cm^{-2}. The model is based on solutions of electron and ion fluid equations describing charged particle transport coupled with Poisson's equation for the electric field. A realistic description of the electron kinetics has been obtained by considering separately two electron groups representing, respectively, the tail and the bulk of the electron distribution function. The validity of the two-electron group fluid model has been checked with Monte Carlo simulations.

I. INTRODUCTION

Capacitively coupled rf glow discharges are widely used in the microelectronics industry as a source of reactive species for plasma etching or deposition. A better understanding of these discharges and the ability to predict their properties for different operating conditions are a prerequisite for a better control of the process.

The development of self-consistent numerical fluid models of rf discharges[1–5] has been useful in clarifying the basic mechanisms occurring in these discharges. The use of these models together with plasma diagnostic techniques has helped to improve our physical description and understanding of the electrical properties of these discharges, and to analyze in detail the discharge properties associated with sheath expansion and contraction, the influence of frequency or the role of negative ions.

In a cold plasma, such as the plasma created by a low-pressure radio-frequency glow discharge, the electrons play a central role by converting the electrical power of the generator into chemical power through excitation, dissociation, and ionization of the gas molecules. Therefore one of the important questions to be addressed in the study of rf glow discharges concerns the mechanisms of electron-energy gain and deposition. These mechanisms determine the space and time variations of the electron velocity distribution function and thus of the production rates of the reactive species, i.e., excited species, and dissociation products.

The aim of this paper is to show, on the basis of a self-consistent fluid model, that depending on the discharge operating point, the mechanisms of electron-energy gain and deposition can change drastically, leading to the existence of very distinctive discharge regimes. These regimes are characterized by very specific properties of the electron kinetics. An important consequence for plasma processing is that the nature of the active species produced by electron impact, the space and time distribution of their production, and therefore the plasma chemistry itself can be very dependent on these discharge regimes.

This is illustrated in the case of helium (3 Torr, frequency in the range 3–9 MHz) where the numerical model predicts, self-consistently and in agreement with experimental results, the existence of two different regimes where, depending on the discharge power, either plasma electrons or secondary electrons emitted by the electrodes under ion bombardment play a dominant role in the energy deposition mechanisms. The existence of these two distinct regimes was shown in the early work of Levitskii,[6] and in a number of more recent works (see, e.g., Refs. 7–12).

The numerical results clearly elucidate the role of the sheath field in the electron-energy gain and deposition mechanisms and in the discharge maintenance. The oscillation of the sheath is responsible for the heating of plasma electrons in the first regime. This regime occurs over the whole range of power when there is no secondary electron emission, and is otherwise dominant for low discharge power. It is specific to rf discharges at

sufficiently high frequencies and has no equivalent in a dc discharge. When the discharge power is high enough and if secondary electron emission is present, another regime takes place where most of the energy deposition is due to electrons emitted by the electrodes and accelerated in the sheaths. This regime leads to the formation of a negative glow plasma externally sustained by high-energy electrons coming from the sheaths, as in a dc discharge. Although the sheath plays a central role in both regimes, the mechanisms by which the electrons gain energy from the sheaths are drastically different in each regime. The *motion of the sheath* (expansion) imparts some energy to the *plasma electrons* in the first regime, while the *rms sheath electric field* provides energy to the *secondary electrons* and determines the occurrence of the second regime. This distinction is more than academic and the knowledge of the differences in the plasma properties of both regimes is fundamental for plasma processing applications.[12]

In the cases considered in this paper, the plasma field is very low and does not contribute to the electron heating. In other conditions (the existence of radial losses due to ambipolar diffusion to the walls, or electronegative gases), the electric field in the plasma might be significant, and its contribution to the overall electron-energy deposition can be dominant. This regime which leads to the formation of a plasma similar to the positive column of a dc discharge will not be discussed in the present paper.

The results presented in this paper and their good agreement with experimental measurements in a large range of conditions (power and frequency) show also that, although the validity domain of a fluid model is necessarily limited, it is possible to build fluid models which can predict reasonably well the main characteristics and trends of a rf discharge in a large subset of the multidimensional domain formed by the discharge parameters (power, pressure, frequency, gas mixture, geometry, and nature of the electrodes).

The validity domain of the model is limited due to the necessary assumptions regarding the charged-particle distribution functions which are inherent to any fluid model. However, this domain can be considerably extended by choosing these assumptions in a proper way and on the basis of known physical properties of the charged-particle transport in the conditions considered. Since the kinetic properties of the plasma electrons which are subjected to low electric fields are drastically different from those of the secondary electrons which are emitted by the electrodes and accelerated in the sheath to high energies,[13] we have considered and treated separately two groups of electrons (plasma electrons and cathode emitted electrons). The fluid model is therefore based on equations describing the transport of plasma electrons, secondary electrons, and ions, coupled with Poisson's equation for the electric field.

The theoretical basis of the model are discussed in Sec. II, including a description of the equations and hypothesis concerning the charged particle transport (Sec. II A) and a brief description of the numerical method (Sec. II B). The results are presented in Sec. III. A description of the different rf discharge regimes based on the numerical results and on comparisons with experimental results is given in Sec. III A. The sustaining and power deposition mechanisms of each regime are discussed in Sec. III B. The properties of plasma potential and current densities are presented in Sec. III C. The validity of the model is discussed in Sec. III D on the basis of comparisons with Monte Carlo simulations.

II. PHYSICAL MODEL

The model described below is a self-consistent electrical model of the discharge. In this model, equations describing the electron and ion transport are coupled to Poisson's equation for the electric field in order to obtain the space and time variations of the charged-particle densities, current densities, and electric field during one cycle of the steady-state rf discharge. The coupling between excited species population and electron kinetics is not considered in this simple approach, i.e., the electrons are supposed to interact with a cold, unchanging, neutral background. The choice of a realistic and simple description of the charged-particle transport is of paramount importance in discharge modeling. This question is discussed below.

A. Two-electron group fluid model: Basic equations and data

In this paper, we use a "fluid" approach to describe the electron and ion transport. Although the validity domain of fluid models is limited due to the assumptions on the charged-particles distribution functions which are implied by any fluid description, these methods are a convenient way of modeling discharges when the charged particles' mean free path is much smaller than the characteristic dimensions of the discharge. On the other hand, particle methods (particle-in-cell or Monte Carlo simulations) are much more time consuming, but at the moment they are the only ones currently available to describe low-pressure regimes.[14–16]

In a fluid model, a finite numbers of moments of the Boltzmann equation in the velocity space are used to describe electron or ion transport. This set of moment equations must be closed by some assumptions as to the charged-particle distribution function. Since the ionization rate (and its space and time distribution) is a fundamental parameter of the discharge, it is important to choose the assumptions of the model in such a way that the ionization mechanisms are described as accurately as possible.

It is well known that in a glow discharge, the ionization in the glow is due to electrons emitted by the cathode and accelerated in the sheath. The ionization process in the glow is nonlocal; i.e., the energy released in this region by fast electrons has been gained in the sheath and not in the glow region. In contrast, in the positive column of a glow discharge the energy gained by the electrons is locally balanced by the energy loss due to collisions. The different physical properties of a negative glow and a positive column plasma are mainly due to the fact that the negative glow plasma can be considered as a non-self-sustained plasma, where external ionization is

provided by electrons coming from the sheath, whereas a positive column is locally a self-sustained plasma.

It is therefore very important in any glow discharge model to account for these two different ionization mechanisms: (i) ionization by electrons emitted by the cathode and accelerated through the sheath and (ii) ionization by electrons heated by the local electric field. Note that the possible existence of nonlocal ionization in the glow had not been included in the model described in Ref. 4; this model was therefore not able to predict the specific properties of negative glow types of plasmas (large plasma density, longitudinal ambipolar diffusion).

A very simple way to include these two different ionization mechanisms in a fluid model is to use the two-electron group model[17,18] defined below and which is used in the present work (similar models have been used in Refs. 19–25).

(i) Fast electrons (beam electrons) are emitted by each electrode under ion bombardment. They are assumed to be forward directed and to form a monoenergetic beam. One beam is considered for each electrode. These electrons are accelerated by the intense electric field in the sheath and release their energy upon entering the plasma region. Secondary electrons created by ionization in the sheath are assumed to belong immediately to the fast-electron group; when ionization takes place in the glow, the electrons are assumed to belong to the second electron group (slow electrons, see below). The transport of fast electrons is described by continuity and energy equations [Eqs. (1) and (2), respectively]. The beams are supposed to release instantaneously their energy in the discharge (the continuity and energy equations of the beam electrons are steady-state equations); this approximation is valid only if the transit time of the beam electrons in the sheath and glow regions is much smaller than the period of the rf field.

(ii) The low-energy electrons (bulk electrons) are created in the glow by ionization by the beam electrons. Another source of bulk electrons results when the beam energy falls below the ionization threshold; the beam electrons then join the low-energy group. The bulk electrons are assumed to be in equilibrium with the electric field and they can gain enough energy from the local electric field to ionize the gas molecules. The kinetics of the low-energy electrons and ions is described by continuity and momentum-transfer equation [Eqs. (3) and (4) for electrons and (5) and (6) for ions]. The momentum-transfer equations for bulk electrons and ions are simplified by neglecting the inertia terms; this approximation is valid only in a collisional regime and leads to the representation of the particle flux by the sum of a drift term and a diffusion term [Eqs. (4) and (6) for bulk electrons and ions, respectively]. The above assumptions concerning the kinetic properties of plasma electrons and ions limit the validity domain of the model to pressure higher than a few tenths of a Torr and frequency less than a few tens of MHz for typical values of the power and gap length in plasma processing.

The transport equations are coupled with Poisson's equation (7) in a one-dimensional, parallel plate geometry with conducting electrodes as in Ref. 4. The following set of coupled nonlinear equations is therefore considered:

$$\frac{\partial(n_{bj}v_{bj})}{\partial x}=S_{bj}^{\text{ion}}+S_{bj}^{\text{out}} \quad (1)$$

$$v_{bj}=s_j\left[\frac{2}{m}\varepsilon_{bj}\right]^{1/2} \quad (j=1,2)$$

$$S_{bj}^{\text{ion}}=\begin{cases}(1-A_j)n_{bj}|v_{bj}|Q_i(\varepsilon_{bj}) & \text{if } \varepsilon_{bj}>\varepsilon_i \quad (j=1,2)\\ 0 & \text{if } \varepsilon_{bj}<\varepsilon_i\ ,\end{cases}$$

$$S_{bj}^{\text{out}}=\begin{cases}-\dfrac{n_{bj}|v_{bj}|}{\lambda_b} & \text{if } \varepsilon_{bj}<\varepsilon_t \quad (j=1,2)\\ 0 & \text{if } \varepsilon_{bj}>\varepsilon_t\ ,\end{cases}$$

$$\frac{\partial\varepsilon_{bj}}{\partial x}=eE-\sum_k\varepsilon_k Q_k(\varepsilon_{bj})-A_j\varepsilon_{bj}Q_i(\varepsilon_{bj}) \quad \text{if } \varepsilon_{bj}>\varepsilon_t \quad (j=1,2)\ , \quad (2)$$

$$\frac{\partial n_e}{\partial t}+\frac{\partial n_e\langle v_e\rangle}{\partial x}=S_{b_1}^{\text{ion}}+S_{b_2}^{\text{ion}}-S_{b_1}^{\text{out}}-S_{b_2}^{\text{out}}+n_e|\langle v_e\rangle|\alpha-rn_en_p\ , \quad (3)$$

$$n_e\langle v_e\rangle=n_eW_e-\frac{\partial(n_eD_e)}{\partial x}\ , \quad (4)$$

$$\frac{\partial n_p}{\partial t}+\frac{\partial n_p\langle v_p\rangle}{\partial x}=S_{b_1}^{\text{ion}}+S_{b_2}^{\text{ion}}+n_e|\langle v_e\rangle|\alpha-rn_en_p\ , \quad (5)$$

$$n_p\langle v_p\rangle=n_pW_p-\frac{\partial(n_pD_p)}{\partial x}\ , \quad (6)$$

$$\frac{dE}{dx}=\frac{|e|}{\varepsilon_0}(n_p-n_e-n_{b_1}-n_{b_2}),\quad \int_0^d E\,dx=-V(d)\ . \quad (7)$$

n_{bj}, n_e, and n_p are, respectively, the beam electron, bulk electron, and positive-ion densities; the subscript j refers to each beam [$j=1$ for the beam initiated on the left electrode, $j=2$ for the right electrode; $s_1=+1$ and $s_2=-1$ in Eq. (1)]. $\langle v_e\rangle$ and $\langle v_p\rangle$ are, respectively, the electron and ion mean velocities parallel to the electric field. S_{bj}^{ion} ($j=1,2$) is the ionization rate of beam j. The parameter A_j is set to zero in the glow region (electrons created in the glow belong to the bulk electron group) and to one in the sheath (electrons created in the sheath belong to the beam electron group). The sheath-glow boundary is supposed to be situated at the point where the electric field is less than a given arbitrary value taken here to be 10 V/cm/Torr. ε_{bj} ($j=1,2$) is the energy of each beam. $Q_k(\varepsilon)=N\sigma_k(\varepsilon)$, where N is the gas density and σ_k the cross section corresponding to the inelastic collisional process k ($k=i$ corresponds to ionization); ε_k is the energy threshold of process k. The sum in Eq. (3) includes all the inelastic processes. As soon as the beam energy becomes lower than the ionization threshold, the beam electrons join the bulk electron group at a rate S_{bj}^{out} characterized by the parameter λ_b (this length parameter is chosen as small as possible, but is finite in order to

avoid discontinuities in the source terms). $n_e|\langle v_e\rangle|\alpha$ is the ionization rate by bulk electrons (α is the ionization coefficient of bulk electrons and is supposed to depend only on the magnitude of the local electric field); r is the electron-ion recombination rate. W_k and D_k are the drift velocity and diffusion coefficient of particles of type k [$W_k=\mu_k E$, where $\mu_k(E)$ is the mobility]. E and V are the local electric field and potential, and d is the gap length.

The boundary conditions for the charged particles are as follows: the densities are set to zero on the electrodes; the flux of electrons emitted by each electrode is given by

$$n_{b_1}v_{b_1}=-\gamma n_p(0)\langle v_p(0)\rangle\ ,\quad n_{b_2}v_{b_2}=-\gamma n_p(d)\langle v_p(d)\rangle\ ,$$

where γ is the secondary electron emission coefficient and $n_p\langle v_p\rangle$ the positive ion flux on the electrode (the above equations hold only when the ion flux is directed toward the electrode, otherwise the flux of emitted electrons is zero); and the mean energy of electrons emitted by the electrodes (under ion bombardment) is equal to 1 eV: $\varepsilon_{b_1}(0)=\varepsilon_{b_2}(d)=1$ eV. The potential waveform between the electrodes is given and assumed to be of the form $V(d)=V_{\rm rf}\cos(\omega t)$, where $\omega=2\pi F$ (F is the frequency).

The results presented below correspond to helium. Electron and positive-ion transport coefficients (drift velocity and ionization coefficient) are taken from Ward.[26] The diffusion coefficient of the bulk electrons has been chosen in such a way that their mean energy is constant and equal to 1 eV. The mean electron energy in the plasma is therefore not calculated self-consistently; this might lead to some uncertainties in the calculation of the plasma density. Electron-ion recombination has been neglected ($r=0$). The inelastic electron-atom cross sections (for the beam-energy equation) are the same as in the work of Boeuf and Marode.[13]

B. Numerical technique

Equations (1)–(7) are integrated in time until a harmonic steady state is reached. Two important points must be carefully considered when developing a numerical method to solve this system: (i) the spatial discretization scheme for the electron and ion transport equations must be able to deal with large density gradients and with fields reversals and (ii) small relative variations of the electron density in the plasma can induce large field variations (if every other parameter is kept constant). In Ref. 4, the time integration of the continuity and Poisson's equations was explicit, i.e., the equations were integrated successively in time. The explicit treatment implies that the electric field is supposed to be constant during the time integration of the electron and ion transport equations; the electric field is adjusted only at the end of the time step. The explicit method is stable only if the time step is limited by (see, for example, Ref. 2)

$$\Delta t<\frac{1}{\frac{|e|}{\varepsilon_0}(n_e\mu_e+n_p\mu_p)}\ . \tag{8}$$

For large plasma densities, this condition may be extremely strong and convergence cannot be reached in a reasonable amount of computational time. Typically, in helium a 1 Torr and for a plasma density of 10^{11} cm^{-3}, the time step must be less than 10^{-11} s for an explicit method. Since the discharge might reach a steady state on the time scale of ms in these conditions, more than 10^8 time integration steps will be necessary.

Considering the above points, our numerical method has been constructed along the following lines: (i) the spatial discretization scheme used for the transport equations [Eqs. (3)–(6)] is the Scharfetter-Gummel exponential scheme, which has proved to be very efficient in the field of semiconductor device modeling,[27] and more recently for discharge modeling.[4,19,21,23,24] (ii) the time integration of the system formed by the charged-particle transport equations and Poisson's equation [Eqs. (3)–(7)] is partly implicit. This is made possible by linearizing the system with respect to the three variables (electron density, ion density, and electric field or potential). This leads to a block tridiagonal linear system which is integrated using standard matrix inversion techniques. Newton iterations are used to achieve convergence within one time step. The time step is no longer limited by condition (8) and can be several orders of magnitudes larger. However, in the case of rf discharges, the time step is still limited by the time variations of the applied potential, and 20 to 100 time steps per cycle has been used in the results presented below (these results have been obtained by following the time variations of the discharge during 10^4 cycles). Note finally that the source terms of the continuity equations [the right-hand side of Eqs. (3) and (5)] have not been linearized, and were supposed to depend on the values of the variables at the end of the previous time step. The transport equations for the beam electrons [Eqs. (1) and (2)] are solved separately at each time step, using a fourth-order Runge-Kutta method. A detailed description of the implicit numerical method can be found in Ref. 28 (in the context of semiconductor device modeling).

III. RESULTS

The results presented in this section have been obtained for the following conditions: helium; pressure; $p=3$ Torr; gap length; $d=3$ cm; frequency; calculations have been performed for three values of the frequency of the applied voltage; $F=3.2$, 6.3, and 9.2 MHz; the amplitude $V_{\rm rf}$ of the applied voltage [$V(d)=V_{\rm rf}\cos(\omega t)$] has been chosen in the range (100–400 V); the electrodes are supposed to be metallic parallel plates; the value of the secondary emission coefficient γ (due to ion bombardment) has been chosen in the range (0.0–0.2). These conditions are close to those used in the experimental work of Godyak and Kanneh[7] except for the gap length, which was 7.8 cm in their experiments. The calculations do not include radial losses which can be important in the experimental conditions of Godyak and Kanneh (the discharge takes place in a 6-cm-diam cylinder). On the other hand, the plasma chemistry is ignored in the calculations and the electrons are assumed to interact with a cold, unchanging neutral background. Comparisons be-

tween the numerical results and the experimental results of Godyak and Kanneh are shown below.

A. Transition between different regimes

The general properties of the rf discharge predicted by the model described above are similar to those obtained with the equilibrium model of Ref. 4 and by other models (Refs. 1–5). The sheaths oscillate periodically on each electrode; at the considered frequencies, the ion density cannot respond to the instantaneous variations of the electric field and its modulation is negligible. The electron density is strongly modulated in the sheaths, and this modulation is related to the sheath contraction and expansion on each electrode successively. The discharge is mainly capacitive (the phase shift between total current and applied voltage is close to $\pi/2$) and the displacement current density in the sheath is much larger than the charged-particle current densities during most of the cycle duration (see Sec. III C).

However, some important features concerning the existence of different discharge regimes where the sustaining mechanisms of the discharge are qualitatively different can only be predicted properly with the two-electron group fluid model used in the present work, in contrast with previous models, such as the one described in Ref. 4 (in this reference, only one-electron group was considered and no distinction was made between the kinetic properties of electrons emitted by the electrodes and bulk electrons). These features are discussed below.

Figure 1 shows the variations of the plasma density (electron density in the center of the plasma) as a function of rf voltage for a discharge in helium ($p=3$ Torr, $d=3$ cm, $\gamma=0.2$) for $F=3.2$, 6.3, and 9.2 MHz. The solid lines correspond to the numerical results, while the dotted lines correspond to the experimental measurements of Godyak and Kanneh[7] (same conditions except for the gap length, which was 7.8 cm in the experiments).

From this figure, it appears that two different regions can be distinguished according to the slope of the plasma density as a function of the rf potential amplitude. Let us first comment on the numerical results. For low applied voltages (from $V_{rf}=100$ V to $V_{rf}\sim 250$ V) the plasma density increases relatively slowly with the rf voltage; in this region, the plasma density increases with frequency for a given rf voltage. In the second region (rf potential larger than 250 V) the slope of the plasma density versus rf voltage is larger by several order of magnitudes, the transition being quite abrupt. Note also that in this region, the plasma density is less sensitive to the value of the discharge frequency. The experimental results display similar features, although the transition between the two regions occurs at higher voltages in the experiments.

These two regions are representative of two different operating regimes of the discharge. These regimes were observed and characterized experimentally a long time ago by Levitskii.[6] More recent publications concerning this question include Refs. 8–12. The low-voltage (or low-power) regime has been qualified as the "α regime" by Levitskii, while the high-voltage regime was referred to as the "γ regime." The physical meaning of these two regimes is discussed below and in the following sections.

The fundamental difference between the two regimes is related to the sustaining mechanism. In the low-power regime the dominant electron-energy gain mechanism is related to the sheath expansion, which imparts periodically some energy to the plasma electrons, while in the higher-power regime the electrons which are responsible for the discharge maintenance and for most of the electron-energy deposition are the electrons emitted by the electrodes under ion bombardment ("γ electrons"), as in the cathode region of a dc glow discharge.

Since the secondary electron emission plays a key role in the transition, it seems interesting to study the effect of the value of the γ coefficient on the shape of the curves plotted in Fig. 1. Figure 2 shows the variations of the

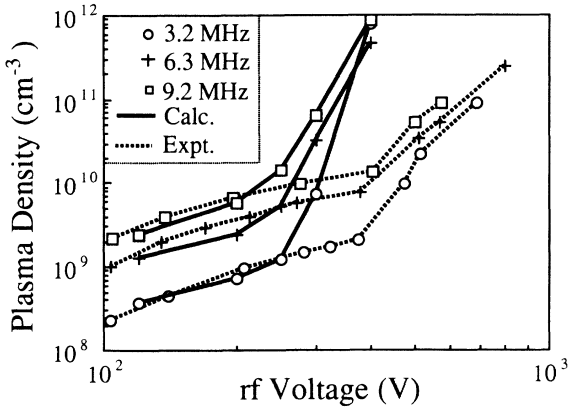

FIG. 1. Variations of the plasma density as a function of the rf voltage amplitude for a discharge in helium ($p=3$ Torr, $d=3$ cm, $\gamma=0.2$) and for three values of the frequency ($F=3.2$, 6.3, and 9.2 MHz). Numerical results (solid lines) and experimental results from Godyak and Kanneh (Ref. 7) (dotted lines) are represented.

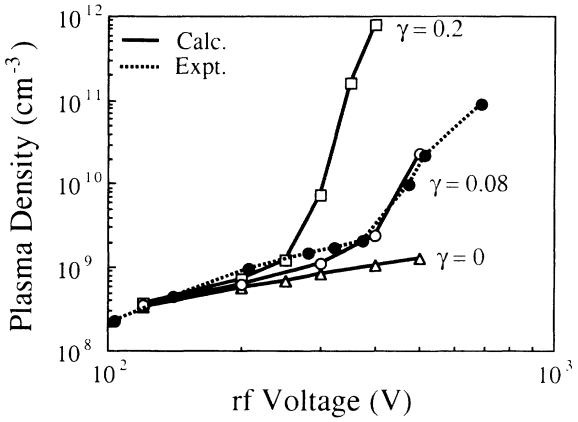

FIG. 2. Variations of the plasma density as a function of the rf voltage amplitude for a discharge in helium ($p=3$ Torr, $d=3$ cm, $F=3.2$ MHz) for three values of the secondary electron emission coefficient ($\gamma=0.0$, 0.08, and 0.2). The experimental results of Godyak and Kanneh (Ref. 7) at 3.2 MHz are also represented.

plasma density versus rf voltage for 3.2 MHz and for three different values of γ; the corresponding experimental result of Godyak and Kanneh[7] is also represented. It appears, from the results shown in this figure, that when γ is set to zero, no transition is observed and the slope of the curve representing the plasma density as a function of the applied voltage stays small in the V_{rf} range considered; the transition voltage decreases when the secondary electron coefficient increases; and best agreement between experimental and numerical results occurs for $\gamma=0.08$.

Although the agreement between experimental and numerical results seems good for $\gamma=0.08$, it must be kept in mind that the accuracy of the plasma density predicted by the model is limited for the following reasons: the electron mean energy in the plasma is not calculated self-consistently, the role of metastable atoms in the overall electron balance is neglected, and radial losses (which can be significant in the experiments of Godyak and Kanneh) are not considered.

The above results show clearly that the observed transition is due to the increasing role of the secondary electrons when the rf voltage or the discharge power increases. The ionization mechanisms in both regimes are described in more detail in the next section.

B. Sustaining and energy deposition mechanisms in the two regimes

In order to avoid any ambiguity or any contradiction with previous work concerning the definition of the two regimes described above, we shall use in the following the term—the "wave-riding regime"—to qualify the regime corresponding to low rf voltage or power, and the term "secondary electron regime" to describe the higher-power regime. A more complete and more accurate definition of these terms will appear in the following.

In order to illustrate the wave-riding mechanism, Fig. 3 shows the space and time variations of the electron density and electric field in the region close to the left electrode immediately after the anodic part of the cycle for this electrode (around $t=0.5$ T). During the anodic part of the cycle the plasma electrons move toward the electrode while the sheath contracts until some of these electrons are absorbed by the electrode. During the following sheath expansion (starting at time t_1 in Fig. 3) the remaining electrons in the region close to the electrode are swept back into the plasma. This motion of the sheath coupled with the electron motion can be seen in Fig. 3. If the sheath expansion is fast enough, i.e., if the frequency is large enough, the cold electrons can gain energy from this expansion and ionize the gas molecules. Assuming that the maximum sheath length (see Fig. 5) does not change very much when the frequency increases from 3.2 to 9.2 MHz (everything else being kept constant), the velocity of the sheath expansion and therefore the ionization efficiency of the wave-riding mechanism must increase. This is coherent with the results shown in Fig. 1 where for a given rf voltage, the plasma density increases when the frequency is changed from 3.2 to 9.2 MHz.

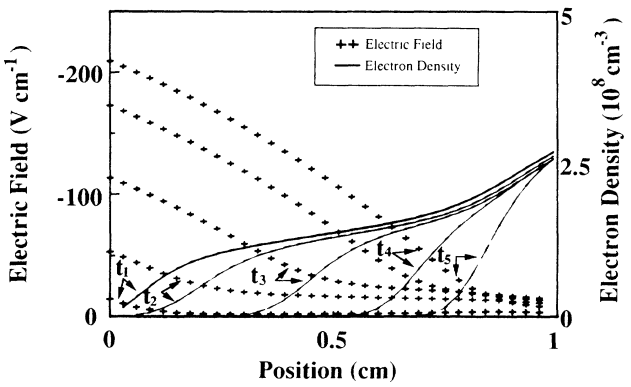

FIG. 3. Spatial variations of the electric field and electron density at five different times during the sheath expansion ($t_1=0.6$ T, $t_2=0.7$ T, $t_3=0.8$ T, $t_4=0.9$ T, $t_5=1$ T) for a discharge in helium ($V_{rf}=120$ V, $F=3.2$ MHz, $d=3$ cm, $p=3$ Torr, $\gamma=0.2$).

Note that the term "wave riding" implies the image of electrons surf riding on the sheath electric field.[9,29] This picture is correct in a collisional equilibrium regime where one can assume that the electron energy gained during the sheath expansion is locally balanced by the loss due to collisions. This assumption, which is implied by our fluid description of the bulk electrons (but not of the cathode emitted electrons), seems reasonable in our case for the two following reasons: (i) The wave riding electrons never "see" the whole sheath voltage since they are pushed by the sheath expansion. The maximum energy they can reach is therefore much smaller than in the case of cathode emitted electrons. (ii) In the conditions considered in Figs. 1–3, the pressure is 3 Torr and the sheath length is of the order of 5–10 mm. The mean free path of low-energy electrons ($\sim$0.2 mm) is therefore much smaller than the sheath length.

However, for lower pressure, the term "wave riding" and the assumption of local equilibrium for bulk electrons are no longer correct. In the low-pressure case, the interaction of the bulk electrons with the sheath is more complex and can be better described in term of reflection by a moving potential wall[30,31] where the electron can either gain or lose energy depending on the direction of motion of the wall (i.e., sheath expansion or contraction).

The secondary electron regime occurs when the contribution of the cathode emitted electrons to the total ionization becomes larger than the contribution of the wave-riding electrons. Figure 4 shows the spatial variations of the ionization rate averaged over one rf cycle for two typical conditions whose operating points ($V_{rf}=120$ and 400 V at 3.2 MHz and $\gamma=0.2$, see Fig. 1) have been chosen in the wave-riding and secondary electron regimes, respectively. The contributions of the bulk electrons and of the secondary electrons to the total ionization are shown separately. It appears that ionization by wave-riding (bulk) electrons is dominant in the first case [Fig. 4(a)], while the contribution of secondary (beam) electrons is much larger in the second case [Fig. 4(b)]. Note that in the secondary electron regime, a non-negligible part of the total ionization takes place within

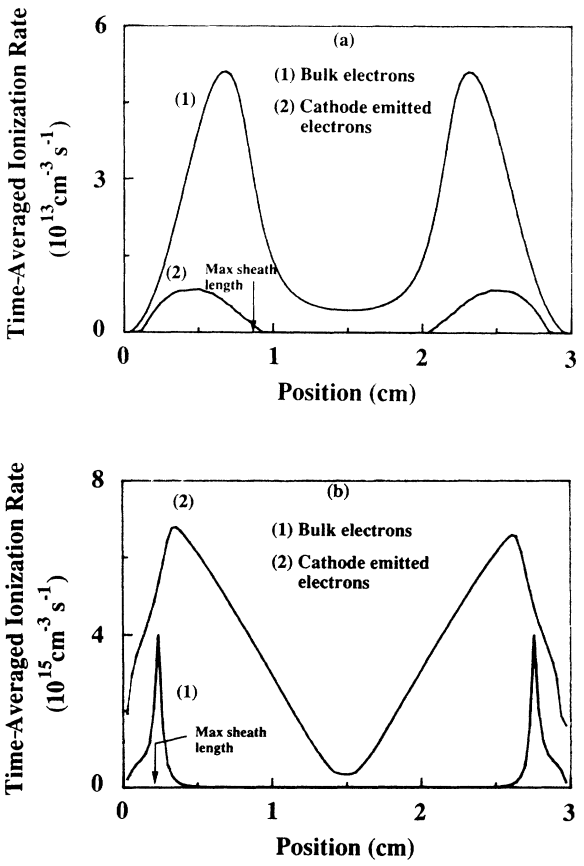

FIG. 4. Spatial variations of the time-averaged ionization rates; the contributions of the secondary (beam) electrons and of the wave-riding electrons are shown separately; (a) helium, $V_{rf}=120$ V, $F=3.2$ MHz, $d=3$ cm, $p=3$ Torr, $\gamma=0.2$; (b) helium, $V_{rf}=400$ V, $F=3.2$, MHz, $d=3$ cm, $p=3$ Torr, $\gamma=0.2$. The positions corresponding to the maximum sheath length are indicated.

the plasma, far from the plasma sheath boundary. The cathode emitted electrons can penetrate deeply into the plasma and release their energy there. In this case, the plasma is similar to the negative glow of a dc glow discharge. The existence of high-energy electrons in the plasma has been shown in a number of experimental works (see, for example, Refs. 32 and 33). Figure 5 presents the space and time variations of the ionization rate for three different values of the applied rf voltage, and illustrates the change in the ionization mechanisms during the transition (similar results have been presented by Okasaki, Makabe, and Yamaguchi[34]). In the case of Fig. 5(a), the dominant ionization mechanism is due to wave-riding electrons. One can see that most of the ionization occurs in the plasma sheath boundary region and only during the sheath expansion. Figure 5(c) illustrates the ionization mechanism in the secondary electron regime. In that case the maximum ionization occurs when the sheath length and sheath potential are maxima. The ionization rate is large in the plasma due to the penetration of high-energy electrons. One can also see some very localized ionization by wave-riding electrons during the

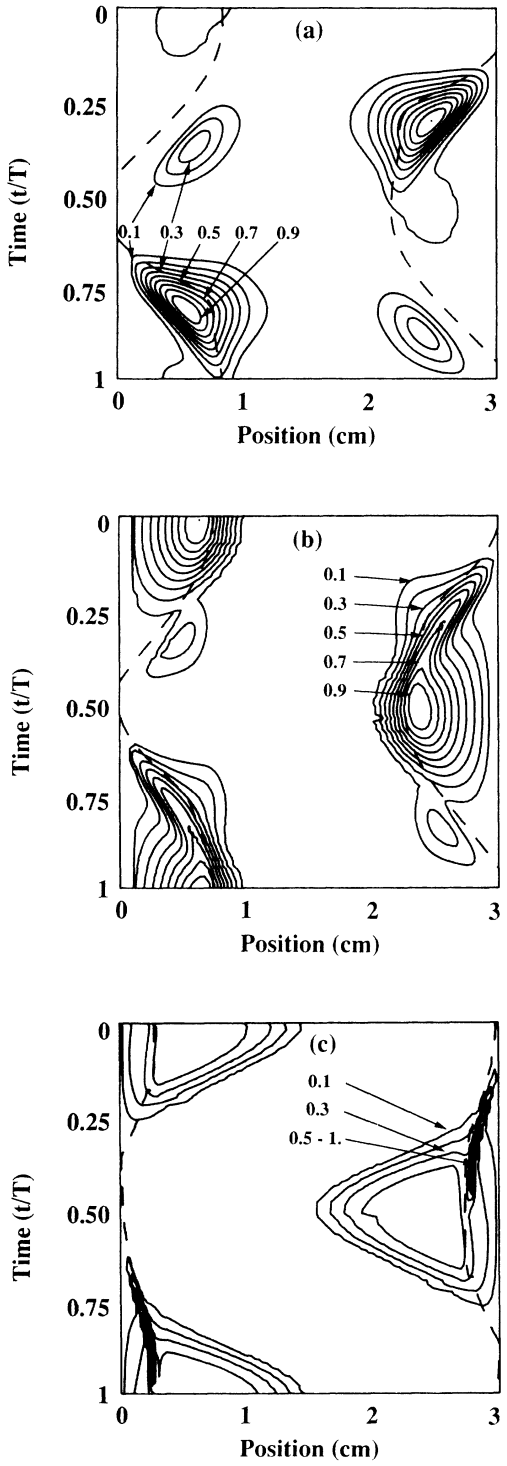

FIG. 5. Contour plots (solid lines) of the space and time variations of the ionization rate for three different discharge conditions showing the transition between the wave-riding regime and the secondary electron regime. The increment between successive contours is constant and equal to 10% of the maximum value of the ionization rate. The dashed line represents a contour of constant electric field magnitude (50 V/cm) and shows the sheath motion. Helium, $F=3.2$ MHz, $d=3$ cm, $p=3$ Torr, $\gamma=0.2$; (a) $V_{rf}=120$ V, unit: 1.3×10^{14} cm$^{-3}s^{-1}$; (b) $V_{rf}=250$ V unit: 5.7×10^{14} cm$^{-3}s^{-1}$; (c) $V_{rf}=400$ V, unit: 1.9×10^{16} cm$^{-3}s^{-1}$.

sheath expansion [note the much shorter sheath length in that case than in Fig. 5(a)]. The rf voltage corresponding to Fig. 5(b) is close to the transition voltage and the two different ionization mechanisms appear clearly in this figure.

Note that in the conditions considered, the electric field in the plasma is very weak and does not contribute to the electron heating. This would not be the case if the radial ambipolar losses to the walls were important, or in the case of an electronegative gas. In such situations, the plasma electric field can be much larger in order to compensate for electron losses (as in a positive column of a dc glow discharge) and its contribution to the overall electron-energy deposition can be dominant[23] (the regime corresponding to this situation must be distinguished from the wave-riding regime or the secondary electron regime where only the sheath electric field contributes to the electron-energy gain).

As can be deduced from Fig, 5, the sheath length decreases abruptly during the transition. The variations of the maximum sheath length and of the total current density in the discharge with the rf voltage are shown in Fig. 6 for two values of the frequency and of the secondary electron emission coefficient. Note, as in Fig. 2, the good agreement of the numerical results for $\gamma=0.08$, with the experimental results of Godyak and Kanneh.[7] The following conclusions can be drawn from this figure: The sheath length decreases much faster with V_{rf} in the secondary electron regime than in the wave-riding regime. This is due to the exponential increase of the ionization rate with the applied voltage in the secondary electron regime, which is related to the fast increase of the plasma density (Fig. 1), current density (Fig. 6), and discharge power (Fig. 7) in this regime; the sheath length decreases with frequency in the wave-riding regime. This decrease is also related to the increase with frequency of

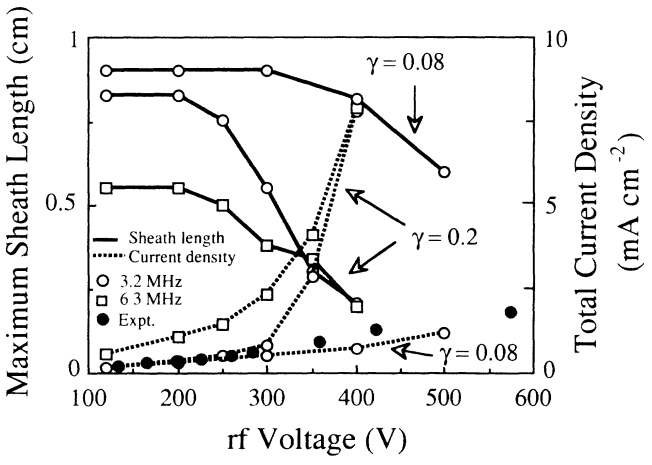

FIG. 6. Variations of the maximum sheath lengths and of the total current density as a function of the rf voltage in helium ($d=3$ cm, $p=3$ Torr) for $\gamma=0.2$, $F=3.2$ and 6.3 MHz, and $\gamma=0.08$, $F=3.2$ MHz; the current density deduced from the experiments of Godyak and Kanneh (Ref. 7) for $F=3.2$ MHz is also represented.

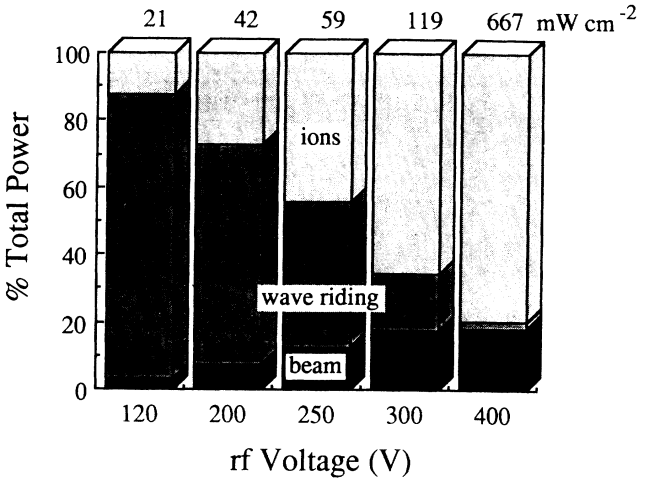

FIG. 7. Partial contributions of the ions, wave-riding (bulk) electrons, and secondary (beam) electrons to the total power deposition for five values of the rf voltage in helium, $F=9.2$ MHz, $d=3$ cm, $p=3$ Torr, $\gamma=0.2$; the total power flux is also indicated.

the ionization rate (and plasma density and total current density); and the total current density and sheath length are less sensitive to the frequency in the secondary electron regime (the discharge "looks like" a dc discharge).

One can expect that, in the secondary electron regime as in a dc discharge, a large part of the discharge power be dissipated by ions in the sheath (or on the electrodes). This is illustrated in Fig. 7, which shows the contribution of the bulk electrons, secondary electrons, and ions to the total energy deposition in the discharge, for different values of the applied voltage. The relative contribution of the bulk electrons is dominant in the wave-riding regime, while most of the energy is dissipated by ions and beam electrons in the secondary electron regime. Note the difference in the magnitude of the total discharge power in the two regimes.

Another important feature of the transition is related to the electron mean energy in the plasma. It has been shown experimentally[7] (see also Ref. 33) that the transition between the wave-riding regime and the secondary electron regime is accompanied by an important decrease in the electron mean energy in the plasma. The low values of the measured electron mean energy (a fraction of an eV) in a rf plasma in the secondary electron regime is characteristic of a negative glow plasma; similar results have been obtained by Den Hartog, Doughty, and Lawler[35] in the negative glow of a dc discharge. Since the mean electron energy of the plasma is not calculated in a self-consistent way, the model cannot predict these properties of the mean electron energy.

We conclude this section by a few comments concerning the transition voltage. The transition voltage can be defined as the voltage for which the contribution of the bulk electrons to the total ionization is equal to the contribution of the secondary electrons. Figure 8 shows the calculated variations with V_{rf} of the space- and time-

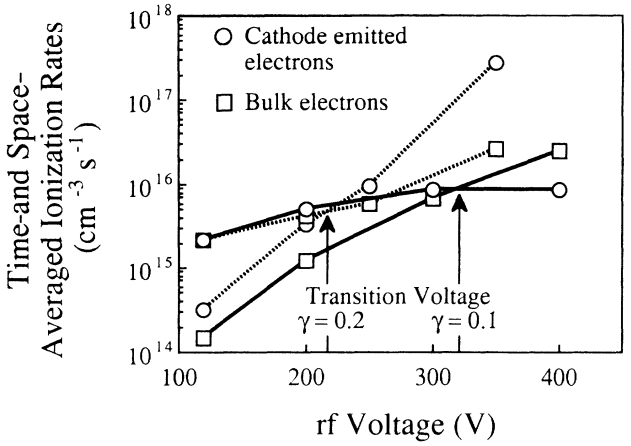

FIG. 8. Time- and space-averaged ionization rates as a function of the applied rf voltage; the contributions of the secondary electrons and of the wave-riding electrons are shown separately. Helium, $F=3.2$ MHz, $d=3$ cm, $p=3$ Torr for $\gamma=0.1$ (solid lines) and $\gamma=0.2$ (dotted lines). The transition voltages are indicated.

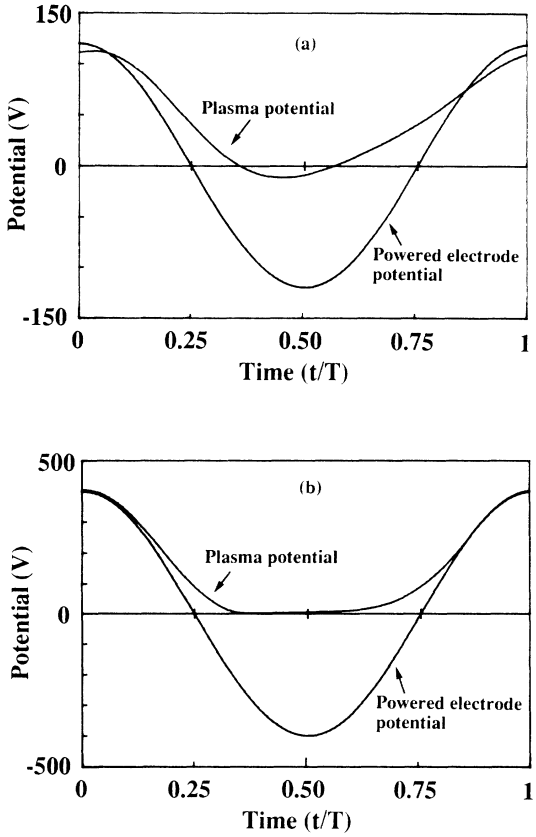

FIG. 9. Time variations of the plasma potential; the potential of the powered electrode is also represented; (a) helium, $F=3.2$ MHz, $d=3$ cm, $p=3$ Torr, $\gamma=0.2$, $V_{rf}=120$ V; (b) same conditions except $V_{rf}=400$ V.

averaged ionization rates of the bulk electrons and secondary electrons for different values of γ at 3.2 MHz. The transition voltages that can be deduced from these curves are $V_{rf}=220$ V for $\gamma=0.2$ and $V_{rf}=330$ V for $\gamma=0.1$. Since the rf discharge in the secondary electron regime is very similar to a dc discharge, one can expect the transition voltage to be related to the minimum operating voltage (normal voltage) of a dc glow discharge. Let us compare the time averaged sheath voltage V_s at the transition to the dc normal voltage. V_s can be roughly approximated by the rms value of the applied voltage ($V_s \sim V_{rf}\sqrt{2}/2$). For $\gamma=0.2$ and 0.1 the calculations give, for the transition, $V_s \sim 160$ and 230 V, respectively. The first value is close to the well known value[36] of the normal cathode fall voltage in helium for an iron cathode. Note that the transition voltage is strongly dependent on the secondary electron emission coefficient. One can therefore estimate the value of γ by comparing numerical and experimental results (cf. Fig. 2) (provided that γ is not strongly dependent on the electric field or the ion energy; see Ref. 35). The larger value of the transition voltage obtained by Godyak and Kanneh[7] seems to indicate that the secondary electron emission in their conditions (titanium electrodes) was close to 0.08.

C. Plasma potential and currents densities

Figure 9 shows the time variations of the plasma potential (defined as the potential in the mid gap) and of the rf potential (potential of the right electrode, the left electrode being grounded) for two conditions typical of the wave-riding [Fig. 9(a)] and secondary electron [Fig. 9(b)] regimes, respectively. The time evolution of the plasma potential predicted by the model is in agreement with previous results.[37]

During the first and fourth quarters of the cycle (Fig. 9), the plasma potential is close to the powered electrode (right electrode, temporary anode) potential because the left electrode is the momentary cathode and most of the potential drop takes place in the cathode sheath. The situation is reversed during the second and third quarters of the cycle where the plasma potential follows the grounded electrode (momentary anode) potential.

Note, however, an important difference between the wave-riding [Fig. 9(a)] and secondary electron [Fig. 9(b)] regimes. In the first case, the plasma potential V_p is lower than the momentary anode potential: at time $t=0$, V_p is less than the right electrode (momentary anode) potential and at $t=T/2$, V_p is less than the left electrode potential (momentary anode). This means that the field tends to draw the electrons to the momentary anode, as in the positive column of a dc discharge. In that case, the drift electron flux as well as the diffusion flux are directed toward the momentary anode. In the secondary electron regime [Fig. 9(b)] the plasma potential is always larger than the potential of both electrodes. This means that the electric field tends to maintain the electrons in the plasma during the whole cycle. The electron flux to the momentary anode must therefore be a diffusion flux (the diffusion flux is larger than the drift flux and in opposite direction). These properties are characteristic of longitu-

dinal ambipolar diffusion accompanied with field reversal in the negative glow of a dc glow discharge.[19,20,24,29,38] Note, finally, that the magnitude of the plasma field is much smaller in the secondary electron regime than in the wave-riding regime (this can be deduced from Fig. 9 by estimating the difference between the plasma potential and the momentary anode potential).

Figure 10 shows the time variations of the total current density and its different components on the left electrode (ion, electron, and displacement) in both regimes. In the wave-riding regime [Fig. 10(a)], the displacement current is much larger than the charged-particle current densities except during the anodic part of the cycle for the left electrode ($t \sim T/2$) where the displacement current couples to the electron current. In the secondary electron regime, the ion current density is a non-negligible part of the total current during the cathodic part of the cycle (the displacement current is still dominant), while the electron current is almost equal to the total current during the anodic part of the cycle. The displacement current goes to zero and changes its sign as soon as the plasma electrons start to flow to the momentary anode ($t \sim T/2$). The change in the sign of the displacement current corresponds to an increase in the magnitude of the electric field in such a way that it limits the electron flow to the momentary anode. The difference between the wave-riding and secondary electron regimes during the anodic part of the cycle is related to the difference in the plasma density and in the nature of the electron flux (drift versus ambipolar diffusion, see above). Note, finally, that in both cases the phase shift between current and voltage is close to $\pi/2$, which is characteristic of a capacitive discharge.

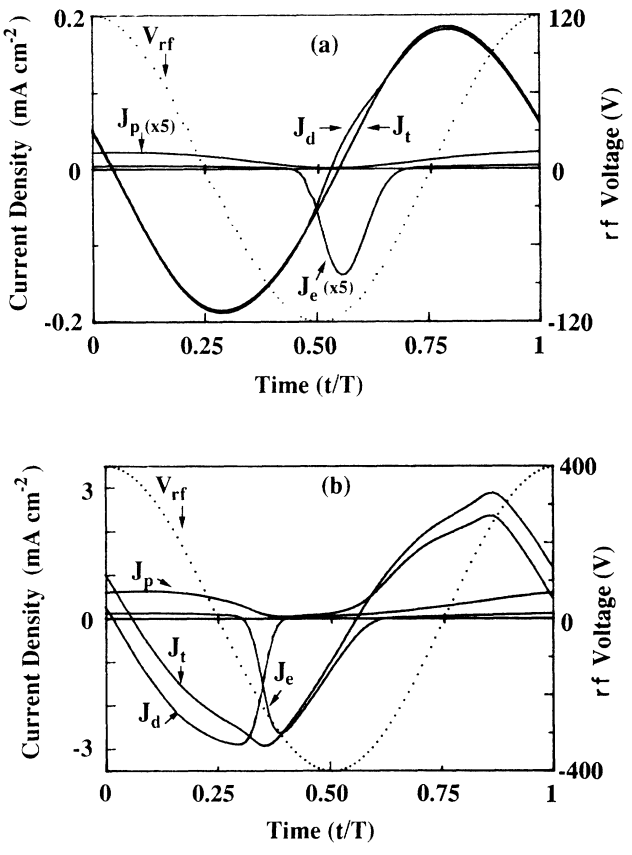

FIG. 10. Time variations of the total current density J_t and of its components (displacement current density J_d, electron current density J_e, positive-ion current density J_p); (a) helium, $V_{rf}=120$ V, $F=3.2$ MHz, $d=3$ cm, $p=3$ Torr, $\gamma=0.2$; (b) helium, $V_{rf}=400$ V, $F=3.2$ MHz, $d=3$ cm, $p=3$ Torr, $\gamma=0.2$. The applied rf voltage is also plotted (dotted line).

D. Validity of the model

The validity of the assumptions concerning the electron-energy distribution function which are implied by the two-electron group fluid model can be checked using Monte Carlo simulations. Although it is difficult to couple directly a Monte Carlo simulation of the charged-particle kinetics with Poisson's equation, it is possible, given the space and time variations of the electric field over one cycle obtained with the self-consistent fluid model for a particular operating point, to solve the electron Boltzmann equation by following the trajectories of the electrons in this space and time varying field. From this microscopic simulations, one can deduce the space and time variations of some macroscopic property of the electrons such as electron density or ionization rate, and compare them with results obtained with the fluid approach. Such comparisons are given in Fig. 11.

Figure 11(a) corresponds to the wave-riding regime ($V_{rf}=120$ V, $F=3.2$ MHz, $d=3$ cm, $p=3$ Torr, $\gamma=0.2$) and shows a comparison between the space and time variations of the electron density obtained with the Monte Carlo simulation (same method as in Ref. 13, extended to time varying situations) and with the fluid model for bulk electrons [Eqs. (3) and (4)]. The calculations start at time $t=0.5$ T, where the electron density is supposed to be uniform in the region limited by the left electrode and the maximum sheath length (electrode emitted electrons are not considered). The electric field is then changed in space and time according to the self-consistent results of the fluid model. The space and time variations of the electron density calculated with both models are compared. The aim of this comparison is to check whether or not the fluid model can provide a realistic description of the wave-riding electrons in a space- and time-dependent electric field. It appears in Fig. 11(a) that the fluid approach and the Monte Carlo simulation give very similar results, although the density profile predicted by the Monte Carlo simulation during the sheath expansion lags behind the density profile predicted by the fluid model by about 1 mm. This discrepancy might be partly due to the neglect of inertia terms in the momentum-transfer equation describing bulk electrons [Eqs. (3) and (4)]: the bulk electrons are assumed to be instantaneously in equilibrium with the local electric field. The agreement between fluid and microscopic results is, however, good enough for our purpose. For lower pressure (as well as for higher frequency), the importance of inertia terms will increase; this is one of the reasons of the nonvalidity of this fluid model at low pressure (the other reasons be-

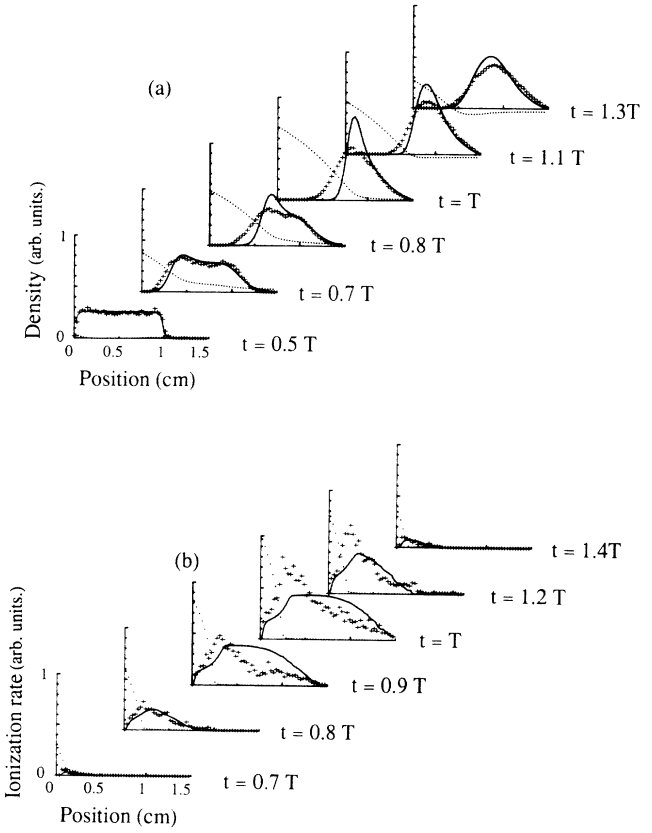

FIG. 11. (a) Time evolution of the electron density profile and electric field during the sheath expansion and contraction in helium, $V_{rf}=120$ V, $F=3.2$ MHz, $d=3$ cm, $p=3$ Torr, $\gamma=0.2$; at time $t=0$ the electron density is assumed to be uniform in the interval defined by the electrode and the maximum sheath length (and zero anywhere else); symbols, Monte Carlo simulations; solid lines, fluid model; dotted line, electric field (the sign of the plotted field is reversed, its maximum absolute value is 220 V/cm). (b) Space and time variations of the ionization rate due to the secondary electrons in helium, $V_{rf}=400$ V, $F=3.2$ MHz, $d=3$ cm, $p=3$ Torr, $\gamma=0.2$; symbols, Monte Carlo results; solid lines, fluid model; dotted line, electric field (the sum of the plotted field is reversed, its maximum absolute value is 2500 V/cm).

ing related to the nonlocality of the electron-energy balance and therefore of the ionization rate).

Figure 11(b) shows a comparison between the ionization rates due to electrode emitted electrons predicted by the fluid model and by the Monte Carlo simulation in the secondary electron regime ($V_{rf}=400$ V, $F=3.2$ MHz, $d=3$ cm, $p=3$ Torr, $\gamma=0.2$) during the sheath expansion and contraction. In these calculations, only electrons emitted by the electrode and their progeny are considered. The time variations of the flux of cathode emitted electrons is taken from the fluid model. The calculations starts at time $t=0.7$ T and the electric field is changed in space and time according to the self-consistent results of the fluid model. The aim of this comparison is to check the ability of the beam model [Eqs. (1) and (2)] to describe the ionization and power deposition by the electrode emitted electrons. From Fig. 11(b) it appears that the beam model provides a reasonably accurate estimation of the space and time variations of the ionization rate by these electrons. However, the penetration depth of these electrons tends to be overestimated by the beam model. This is due to the assumption that the beam electrons are forward directed and that momentum losses are neglected. The beam model is still far better than an equilibrium model, which would predict that all the ionization by these electrons occurs in the sheath. One can therefore conclude that, although the two-electron group fluid model is not perfectly accurate, it contains most of the physical properties of the electron transport in the sheath region.

Let us now briefly discuss the validity of the description of the ion kinetics. The ions are described, as the plasma electrons, by a continuity equation and a simplified momentum-transfer equation [Eqs. (5) and (6)]. This treatment assumes that the ions are instantaneously in equilibrium with the local electric field. This assumption is correct provided that the sheath length is much larger than the ion mean free path and that the mean free time between collisions is much smaller than the characteristic time of the change in the electric field. Given the pressure (3 Torr) and sheath length (larger than 0.3 cm) in our conditions, the assumption of a collisional sheath for ions is correct.[39] However, due to the low ion velocity, the collision frequency for ion-neutral charge exchange is not very large with respect to the frequency of the applied voltage; typically, the ions undergo only a few collisions per cycle with the neutral species. The term involving the time derivative of the ion flux which has been neglected in the ion momentum-transfer equation [Eq. (6)] might therefore be significant. The consequence of this neglect is that the ion velocity (and therefore the ion flux) deduced from the model is more modulated than it should be. On the other hand, this neglect should not have important consequences on the self-consistent determination of the electric field. A simple way to include the inertia term in the ion momentum-transfer equation is to use an effective field as has been done by Richards, Thompson, and Sawin.[3]

IV. CONCLUSION

A self-consistent fluid model of rf glow discharges has been developed. This model is based on equations describing electron and ion transport coupled with Poisson's equation for the electric field. The description of the electron kinetics has been improved with respect to our previous model[4] by considering separately two groups of electrons whose kinetic properties are extremely different: the plasma bulk electrons which gain energy from the sheath expansion, and the electrode emitted electrons which are accelerated by the sheath electric field to high energies and present a beamlike behavior.

The model predicts, in good agreement with experimental results, the existence of two discharge regimes where either the bulk electrons (wave-riding regime) or the beam electrons (secondary electron regime) play the most important role in the electron-energy deposition.

The wave-riding regime corresponds to low discharge power, while the secondary electron regime takes place when the discharge power is increased in such a way that the rms voltage is close to the normal voltage of a dc glow discharge in the same conditions. The numerical results show clearly the similarity of the rf discharge in the secondary electron regime with a dc discharge: in both cases, the plasma adjacent to the sheath has the characteristic property of a negative glow plasma (longitudinal ambipolar diffusion). In the wave-riding regime as well as in the secondary electron regime, the sheath electric field provides most of the electron energy. The way the electrons are heated by the sheath field is, however, different in each case: the electron-energy gain in the wave-riding regime is directly related to the sheath expansion and to the velocity of the sheath motion, while the total electron-energy gain in the secondary electron regime is associated with the time-averaged electric field in the sheath. In the conditions considered in this paper the plasma field does not contribute to the overall electron heating. The role of the plasma field might be much more important in long discharge tubes where radial losses are significant, or in electronegative gases.

Due to the assumptions concerning the charged-particle kinetics, the validity domain of the model is restricted to intermediate pressure (more than a few tenths of a Torr) and to frequency less than a few tens of MHz. Comparisons with experimental measurements and results from Monte Carlo simulations within this range of pressure and frequency confirms the validity of the model. The model can be improved and extended to slightly lower pressure by including an energy equation for the bulk electrons and by considering the inertia terms of the momentum-transfer equations for ions and bulk electrons.

ACKNOWLEDGMENTS

This work has been supported by Groupement de Recherches Coordonnées No. 57 du Centre National de la Recherche Scientifique, NATO and Direction des Recherches et Etudes Techniques, Contract No. 88-108. The authors would like to thank H. Debontride, J. Derouard, R. A. Gottscho, J. Perrin, L. C. Pitchford, and N. Sadeghi for their interest in this work and for a number of valuable discussions and comments. Centre de Physique Atomique de Toulouse is Unité de recherche associé au Centre National de la Recherche Scientifique No. 277.

[1]D. B. Graves and K. F. Jensen, IEEE Trans. Plasma Sci. **PS-14**, 78 (1986); D. B. Graves, J. Appl. Phys. **62**, 88 (1987).

[2]M. S. Barnes, T. J. Cotler, and M. E. Elta, J. Appl. Phys. **61**, 81 (1987).

[3]A. D. Richards, B. E. Thompson, and H. H. Sawin, Appl. Phys. Lett. **50**, 492 (1987).

[4]J. P. Boeuf, Phys. Rev. A **36**, 2782 (1987).

[5]T. Makabe, in *Proceedings of the Ninth ESCAMPIG, Lisbon, 1988,* edited by C. M. Ferreira (European Physical Society, Erice, 1988), p. 277.

[6]S. M. Levitskii, Zh. Tekh. Fiz. **27**, 1001 (1957) [Sov. Phys. Tech. Phys. **2**, 887 (1958)].

[7]V. A. Godyak and A. S. Kanneh, IEEE Trans. Plasma Sci. **PS-14**, 112 (1986).

[8]N. A. Yatsenko, Zh. Tekh. Fiz. **50**, 2480 (1980) [Sov. Phys. Tech. Phys. **25**, 1454 (1980)].

[9]M. J. Kushner, IEEE Trans. Plasma Sci. **PS-14**, 188 (1986).

[10]Y. P. Raizer and M. N. Schneider, Sov. J. Plasma Phys. **13**, 267 (1987).

[11]P. Vidaud, S. M. A. Durrani, and D. R. Hall, J. Phys. D **21**, 57 (1988).

[12]J. Perrin, P. Roca i Cabarrocas, B. Allain, and J. M. Freidt, Jpn. J. Appl. Phys. **27**, 2041 (1988).

[13]J. P. Boeuf and E. Marode, J. Phys. D **15**, 2169 (1982).

[14]R. W. Boswell and I. J. Morey, Appl. Phys. Lett. **52**, 21 (1988).

[15]M. Surrendra, D. B. Graves, and I. J. Morey (unpublished).

[16]K. Kitamori and H. Tagashira, in *Proceedings of the Ninth ESCAMPIG* (Ref. 5), p. 333.

[17]J. H. Ingold, in *Gaseous Electronics,* edited by M. N. Hirsch and H. J. Oskam (Academic, New York, 1978), Vol. 1, p. 19.

[18]A. P. Phelps, B. M. Jelenkovic, and L. C. Pitchford, Phys. Rev. A **36**, 5327 (1987).

[19]J. P. Boeuf and P. Ségur, in *Interactions Plasmas Froids Matériaux,* edited by C. Lejeune (Les Editions de Physique, Les Ulis, 1988), p. 113.

[20]R. A. Gottscho, A. Mitchell, G. R. Scheller, N. L. Schryer, D. B. Graves, and J. P. Boeuf, in *Proceedings of the Seventh Symposium Plasma Proc. Electrochemical Society, Pennington, NJ, 1988,* edited by G. S. Mathad, G. C. Schwartz, and D. W. Hess (Electrochemical Society, Pennington, NJ, 1988), Vol. 22, p. 1.

[21]H. Debontride, J. Derouard, P. Edel, R. Romestain, N. Sadeghi, and J. P. Boeuf, Phys. Rev. A **40**, 5208 (1989).

[22]T. J. Sommerer, J. E. Lawler, and W. N. G. Hitchon, J. Appl. Phys. **64**, 1775 (1988).

[23]J. P. Boeuf and Ph. Belenguer, in *Non Equilibrium Processes in Partially Ionized Gases, NATO Advanced Study Institute, Series B: Physics,* edited by M. Capitelli and J. N. Bardsley (Plenum, New York, in press).

[24]J. P. Boeuf, in *The Physics and Applications of High Power Hollow Cathode Electrode Glow Switches, NATO Advanced Research Workshop,* edited by M. Gundersen (Plenum, New York, in press).

[25]M. Surendra, D. B. Graves, and G. M. Jellum, (unpublished).

[26]A. L. Ward, J. Appl. Phys. **33**, 2789 (1962).

[27]H. K. Gummel, IEEE Trans. Electron Devices **ED-30**, 1097 (1964); see also D. L. Sharfetter, H. K. Gummel, *ibid.* **ED-16**, 64 (1969).

[28]M. Kurata, *Numerical Analysis for Semiconductor Devices* (Heath, Lexington, 1982).

[29]B. Chapman, *Glow Discharge Processes,* (Wiley, New York, 1980).

[30]O. A. Popov and V. A. Godyak, J. Appl. Phys. **57**, 53 (1985).

[31]C. G. Goedde, A. J. Lichtenberg, and M. A. Lieberman, J. Appl. Phys. **64**, 4375 (1988).

[32]G. A. Hebner and J. T. Verdeyen, IEEE Trans. Plasma Sci. **PS-14**, 132 (1986).

[33]G. A. Hebner, J. T. Verdeyen, and M. J. Kushner, J. Appl.

Phys. **63**, 2226 (1988).
[34]K. Okazaki, T. Makabe, and Y. Yamaguchi, Appl. Phys. Lett. **54**, 1742 (1989).
[35]E. A. Den Hartog, D. A. Doughty, and J. E. Lawler, Phys. Rev. A **38**, 2471 (1988).
[36]A. von Engel, *Ionized Gases* (Clarendon, Oxford, 1965).
[37]K. Köhler, J. W. Coburn, D. E. Horne, and E. Kay, J. Appl. Phys. **57**, 59 (1985).
[38]R. A. Gottscho, A. Mitchell, G. R. Scheller, Y. Y. Chan, and D. B. Graves, Phys. Rev. A **40**, 6407 (1989).
[39]J.E. Lawler, Phys. Rev. A **32**, 2977 (1985).

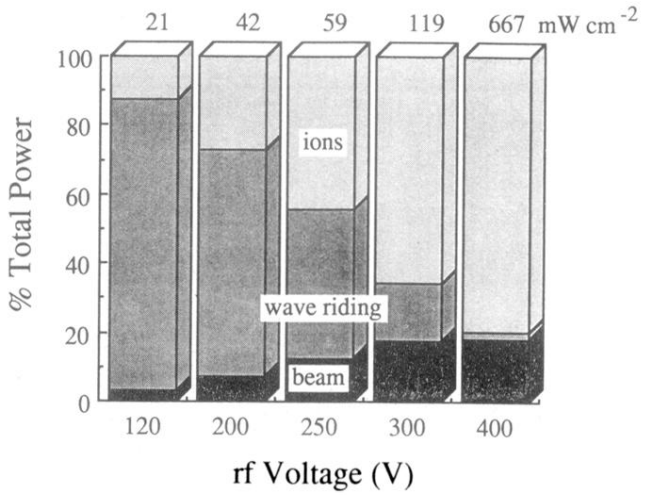

FIG. 7. Partial contributions of the ions, wave-riding (bulk) electrons, and secondary (beam) electrons to the total power deposition for five values of the rf voltage in helium, $F=9.2$ MHz, $d=3$ cm, $p=3$ Torr, $\gamma=0.2$; the total power flux is also indicated.